Supporting Information

CdS-POM nanosheet for highly efficient visible-light-driven H_2 evolution

Wen-Xiong Shi,[a] Zhi-Yong Liu,[a] and Zhi-Ming Zhang,*[a]

[1]Institute for New Energy Materials and Low Carbon Technologies, School of Materials Science & Engineering, Tianjin University of Technology, Tianjin 300384, China

Table of Contents

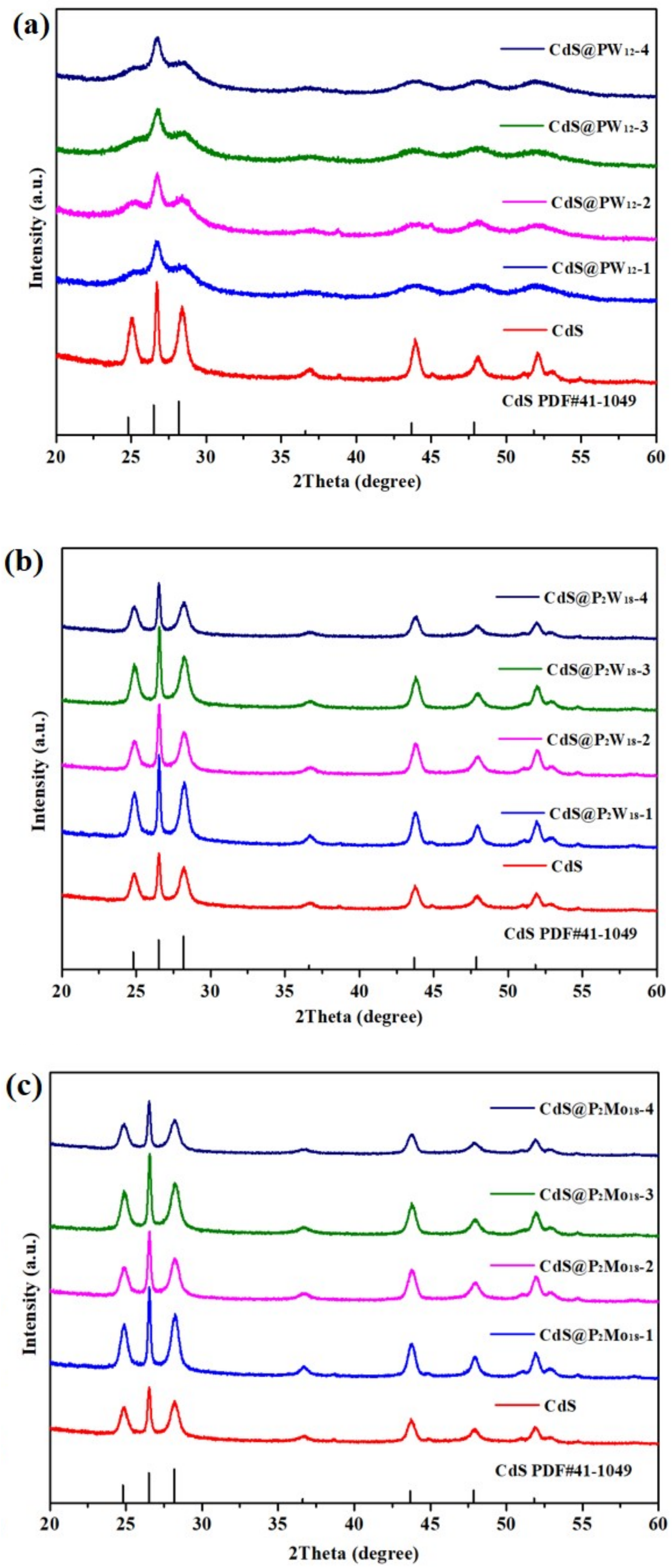

Figure S1. XRD patterns of the different POM doped into CdS. (a) XRD patterns of CdS@PW_{12} composite photocatalysts. (b) XRD patterns of CdS@P_2W_{18} composite photocatalysts. (c) XRD patterns of CdS@P_2Mo_{18} composite photocatalysts.

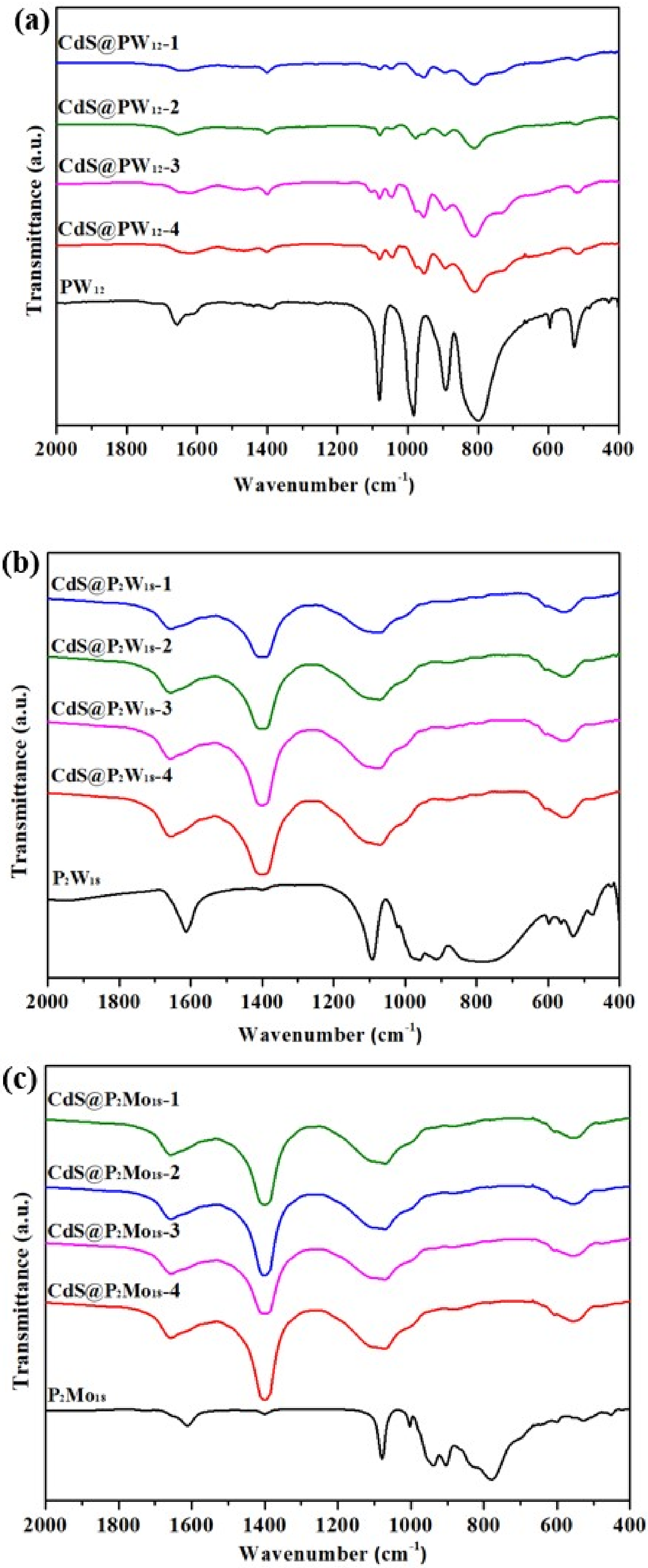

Figure S2. (a) FT-IR spectra of $CdS@PW_{12}$ composite photocatalysts. (b) FT-IR spectra of $CdS@P_2W_{18}$ composite photocatalysts. (c) FT-IR spectra of $CdS@P_2Mo_{18}$ composite photocatalysts.

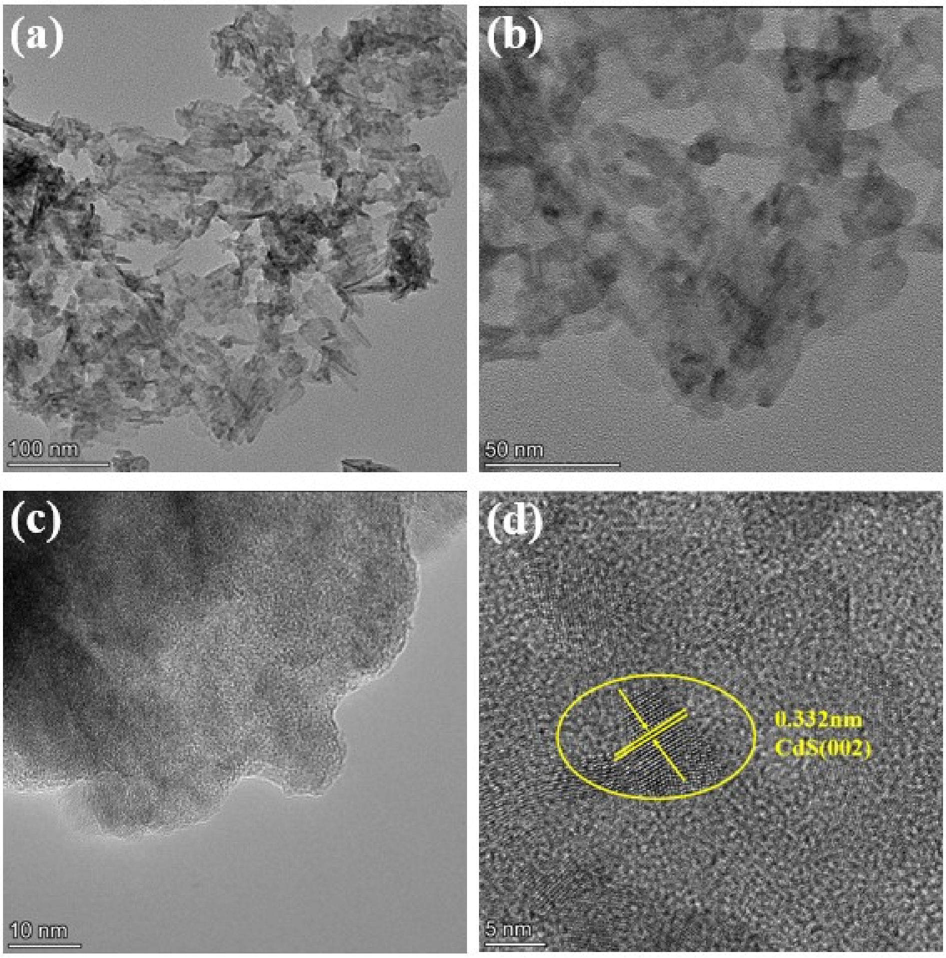

Figure S3. (a) TEM of CdS and (b-d), HRTEM images of CdS.

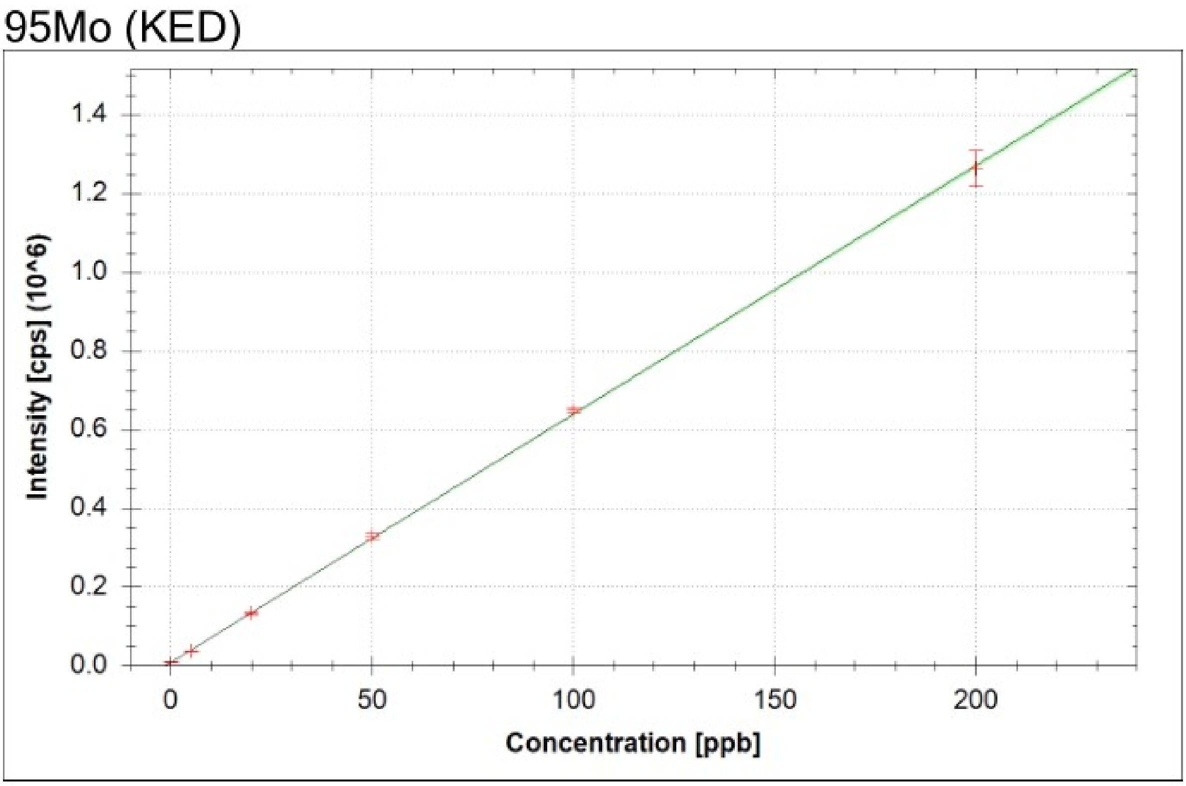

f(x) = 6314.5539*x + 7972.5991

$R^2 = 0.9999$

BEC = 1.263 ppb

LoD = 0.2354 ppb

Figure S4. Calibration curves of Mo elements for ICP-MS.

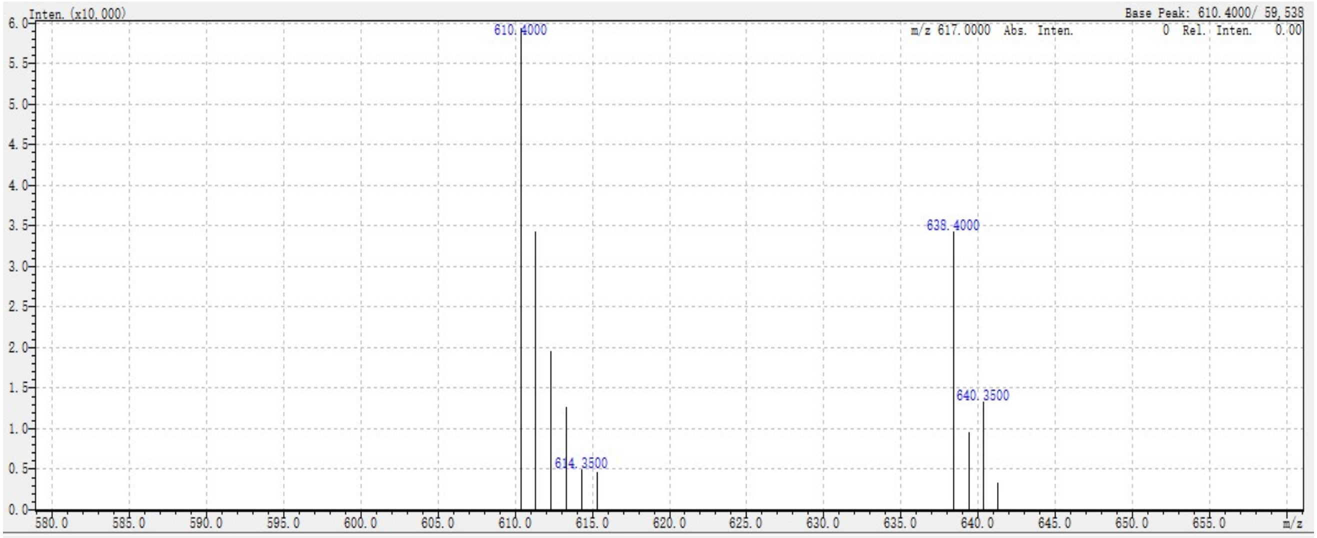

Figure S5. ESI-MS spectrum of PMo_{12}.

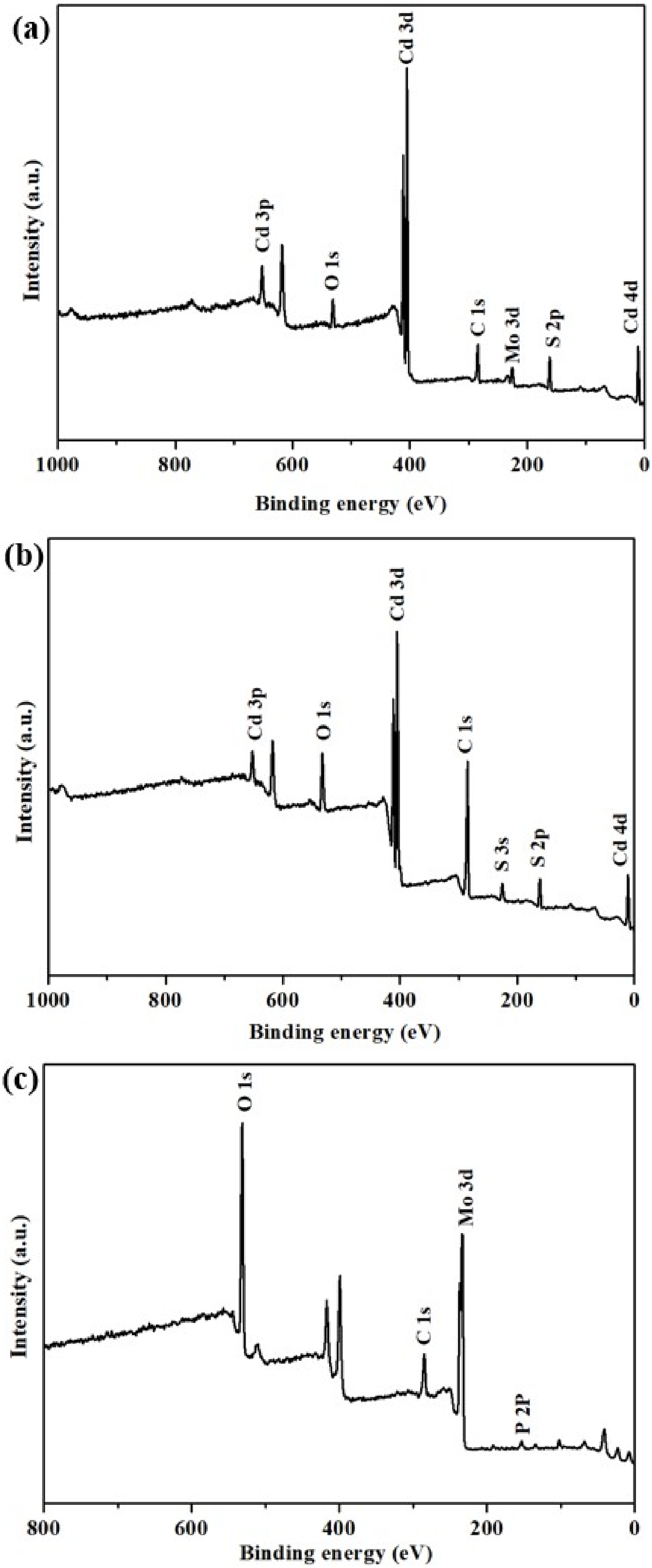

Figure S6. (a) The XPS survey spectrum of CdS@PMo_{12}-3. (b) The XPS survey spectrum of CdS. (c) The XPS survey spectrum of PMo_{12}.

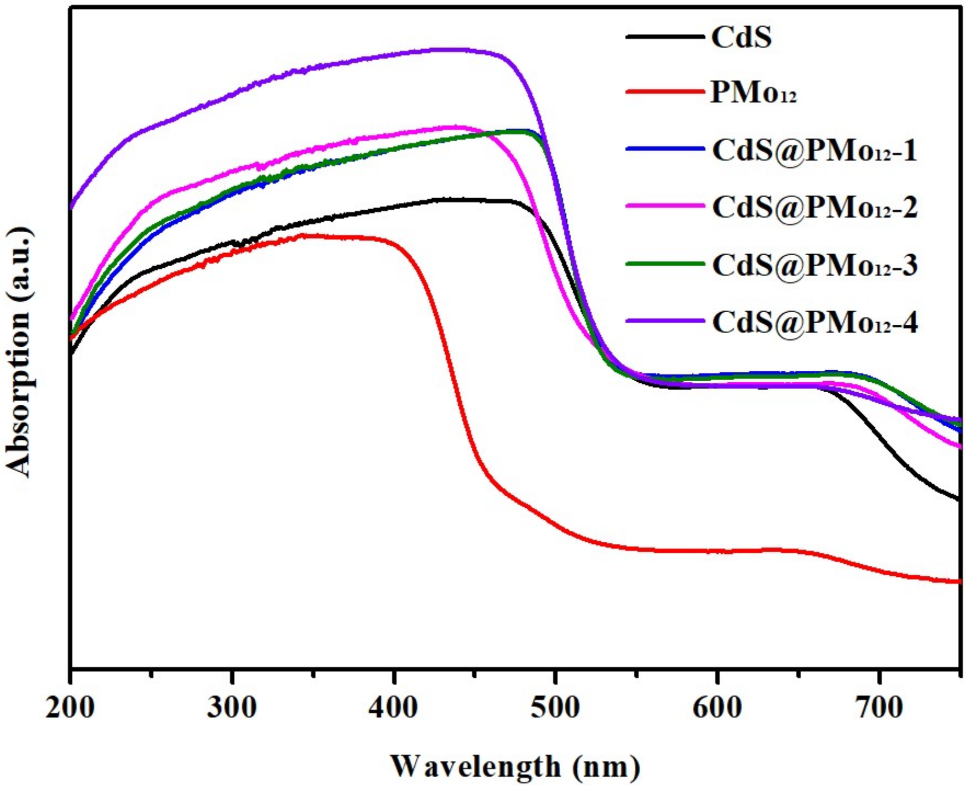

Figure S7. Ultraviolet–visible diffuse reflectance spectra of CdS, PMo_{12} and CdS@PMo_{12}.

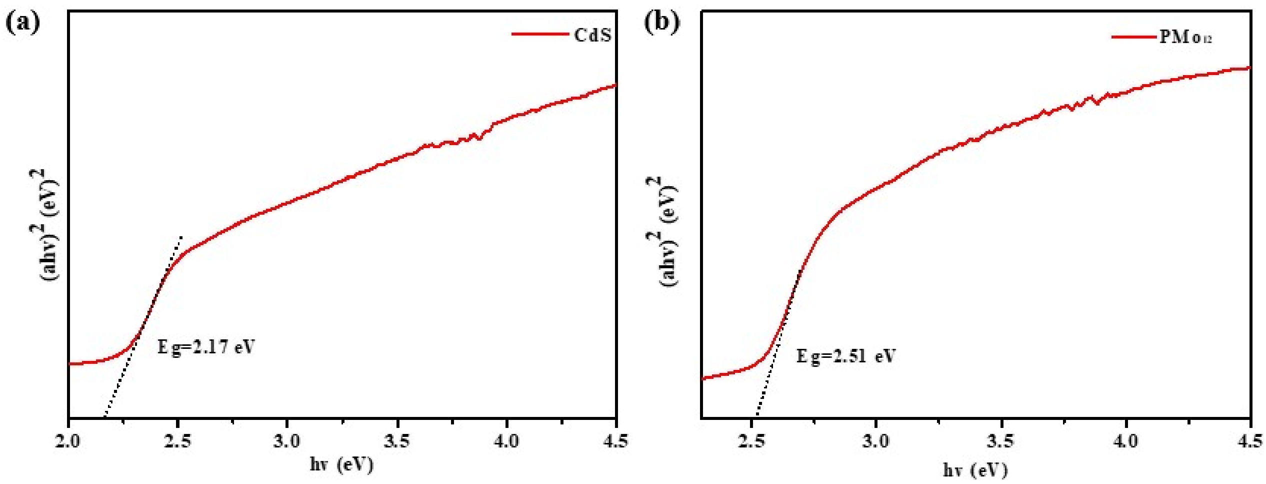

Figure S8. (a) Band-gap calculation of CdS. (b) Band-gap calculation of PMo_{12}.

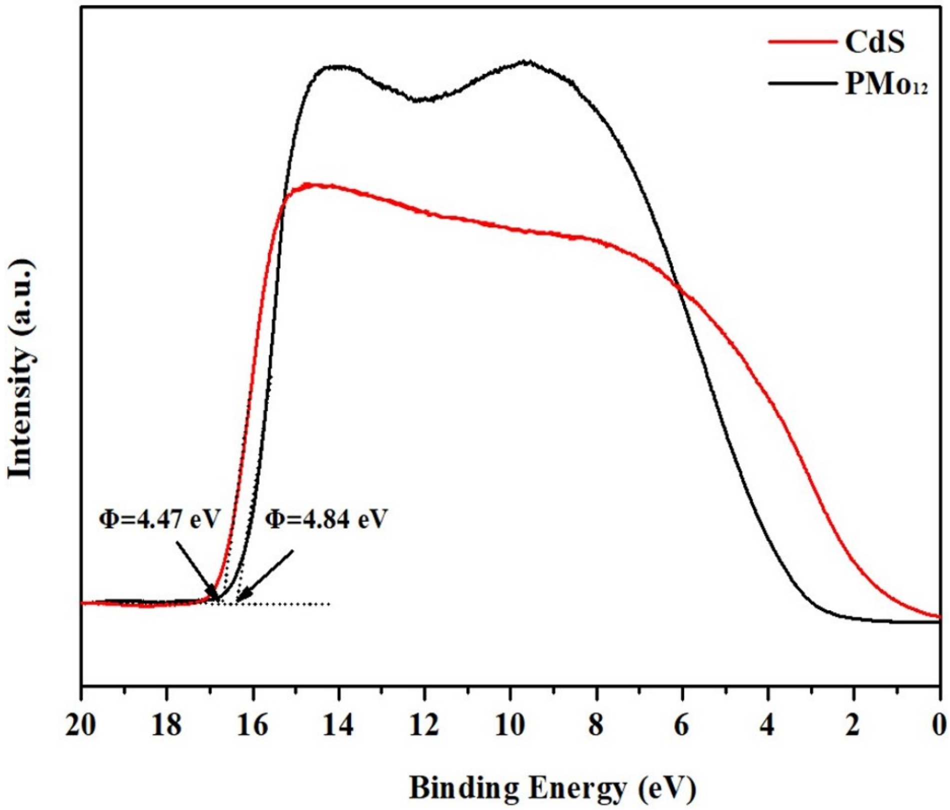

Figure S9. UPS spectra of CdS and PMo_{12}.

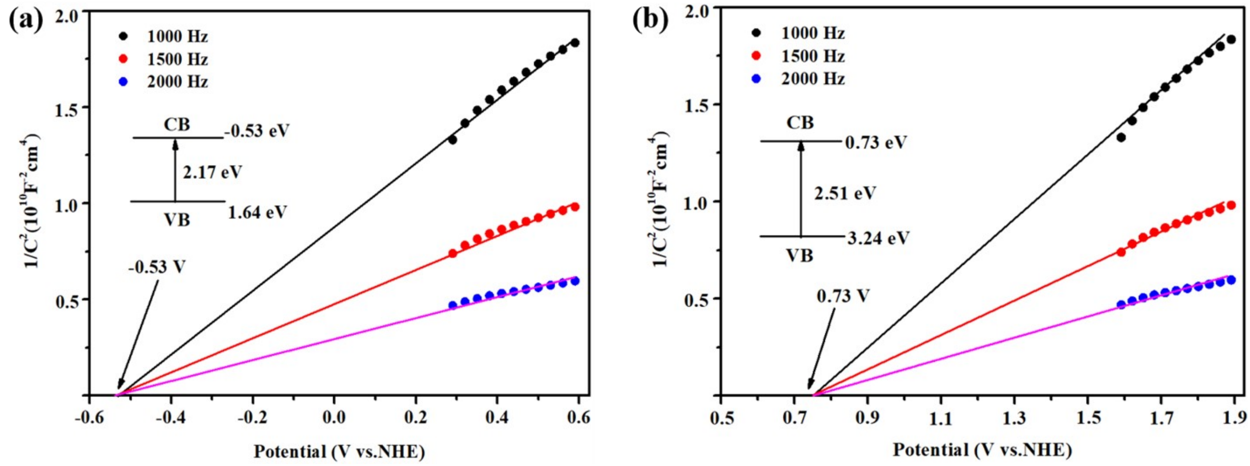

Figure S10. (a) Mott-Schottky diagram of CdS. (b) Mott-Schottky diagram of PMo_{12}.

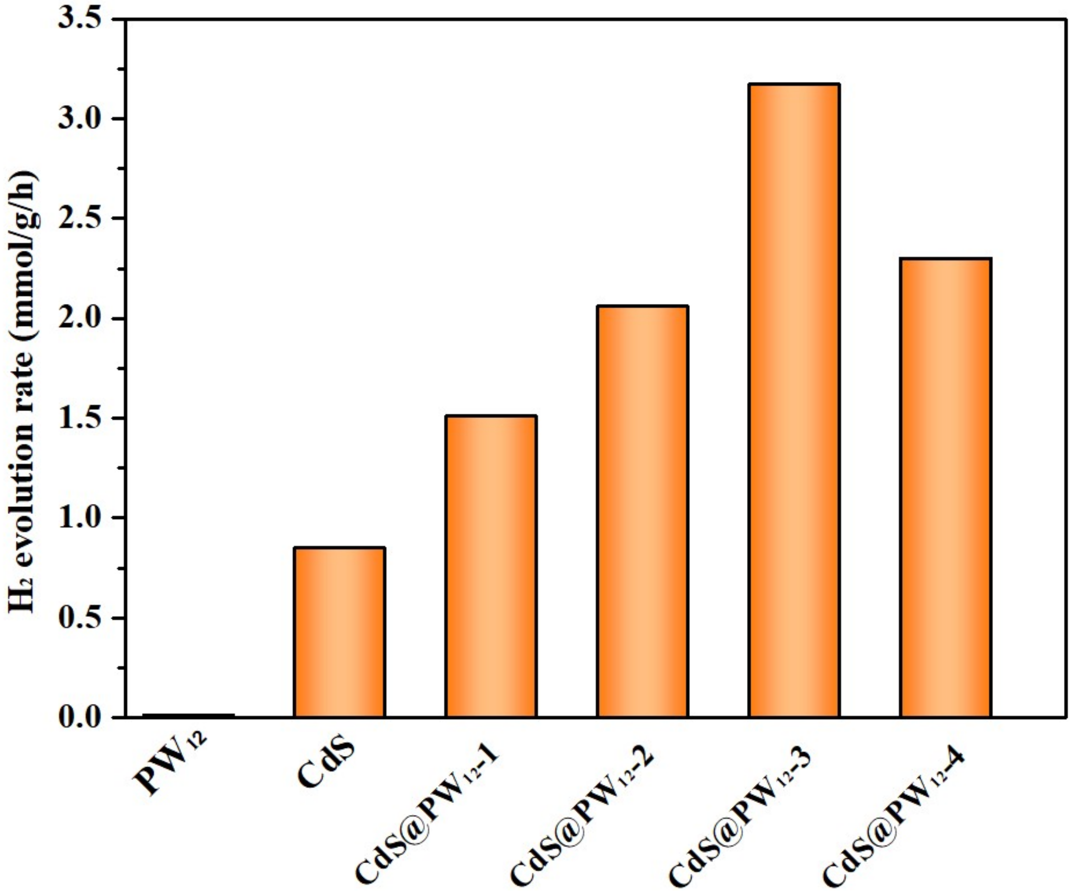

Figure S11. A comparison of the visible-light-driven H_2 evolution rates based on CdS, PW_{12} and CdS@PW_{12} as photocatalysts (λ > 420 nm).

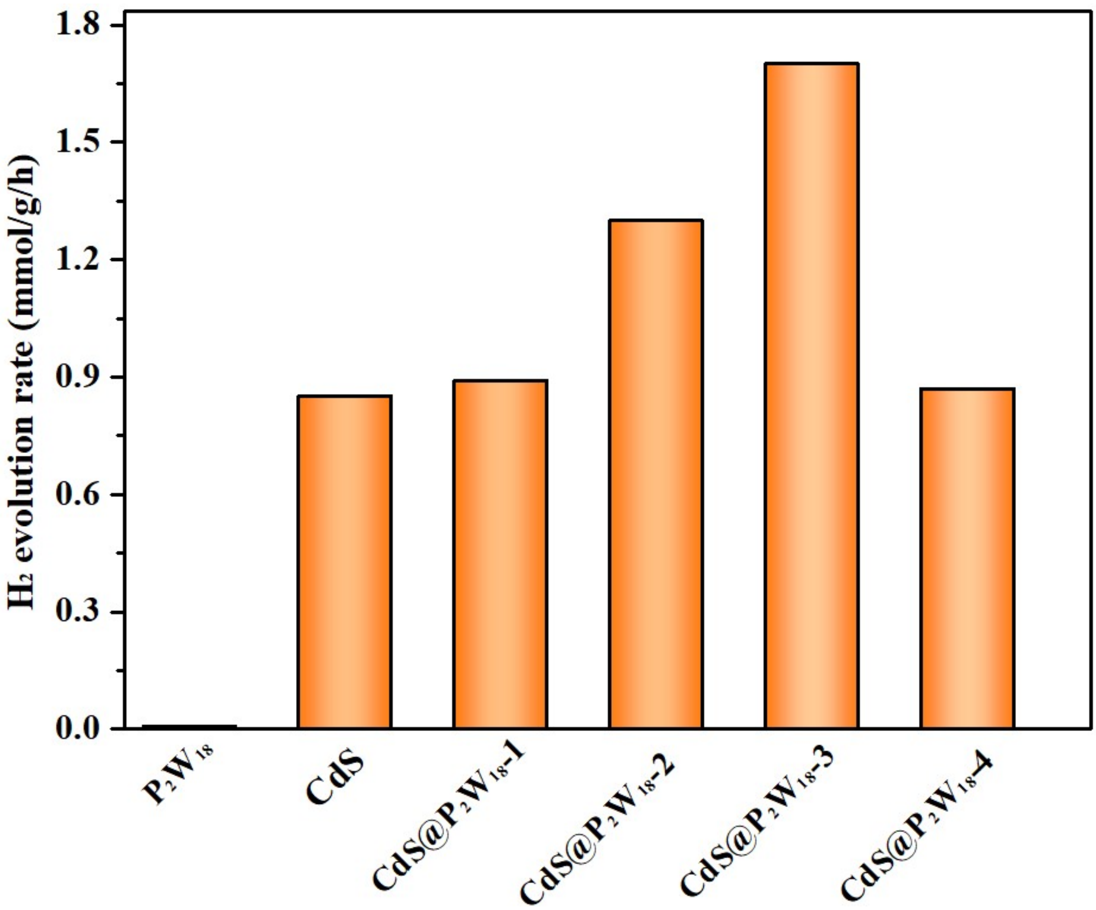

Figure S12. A comparison of the visible-light-driven H_2 evolution rates based on CdS, P_2W_{18} and CdS@P_2W_{18} as photocatalysts ($\lambda > 420$ nm).

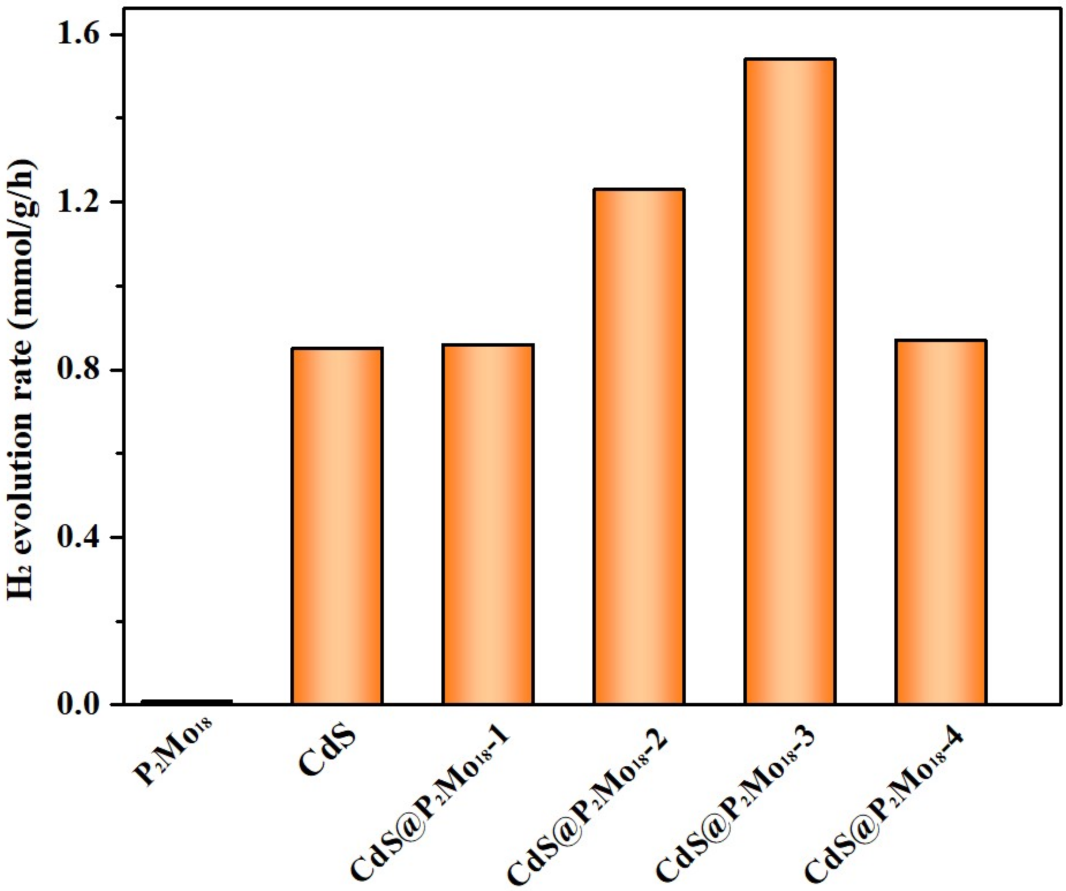

Figure S13. A comparison of the visible-light-driven H_2 evolution rates based on CdS, P_2Mo_{18} and CdS@P_2Mo_{18} as photocatalysts (λ > 420 nm).

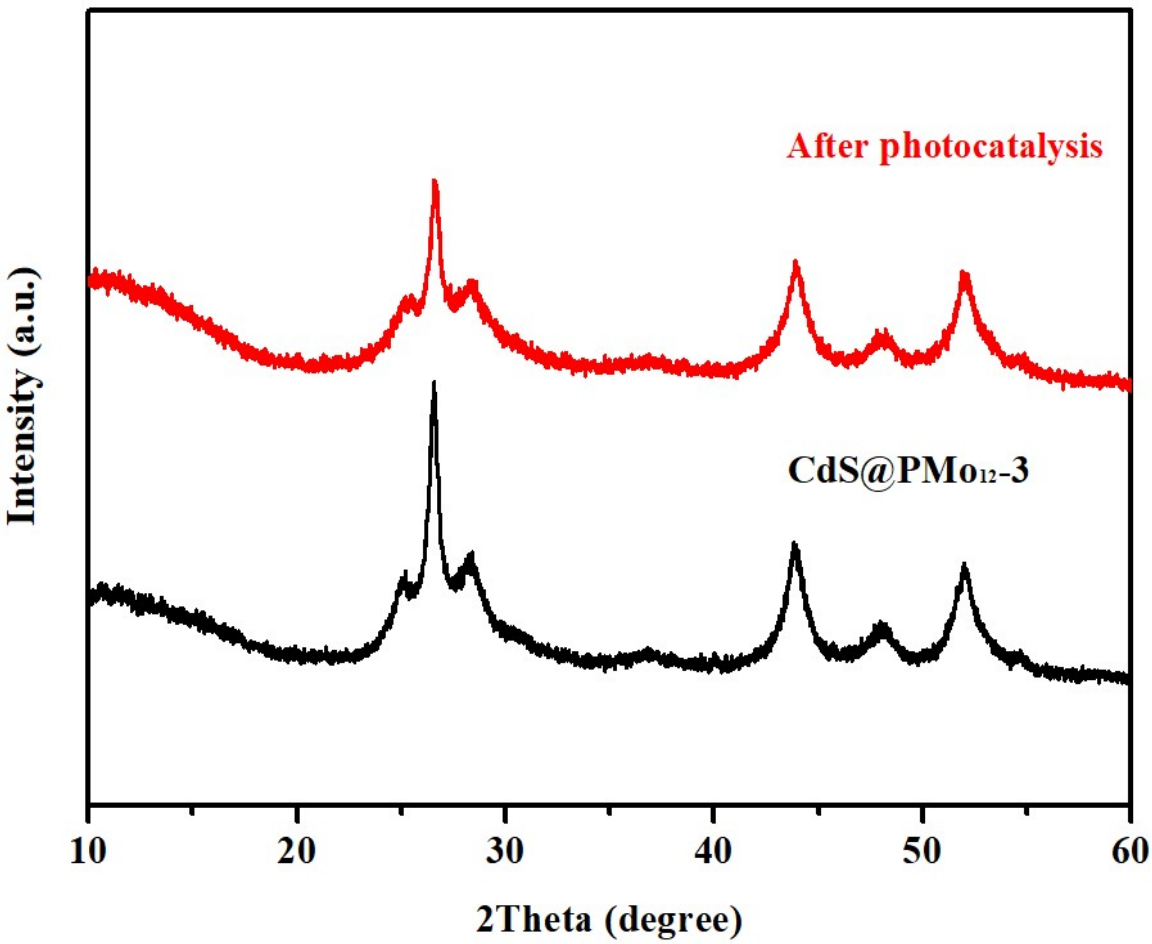

Figure S14. PXRD patterns of CdS@PMo_{12}-3 before and after the photocatalytic H_2 evolution.

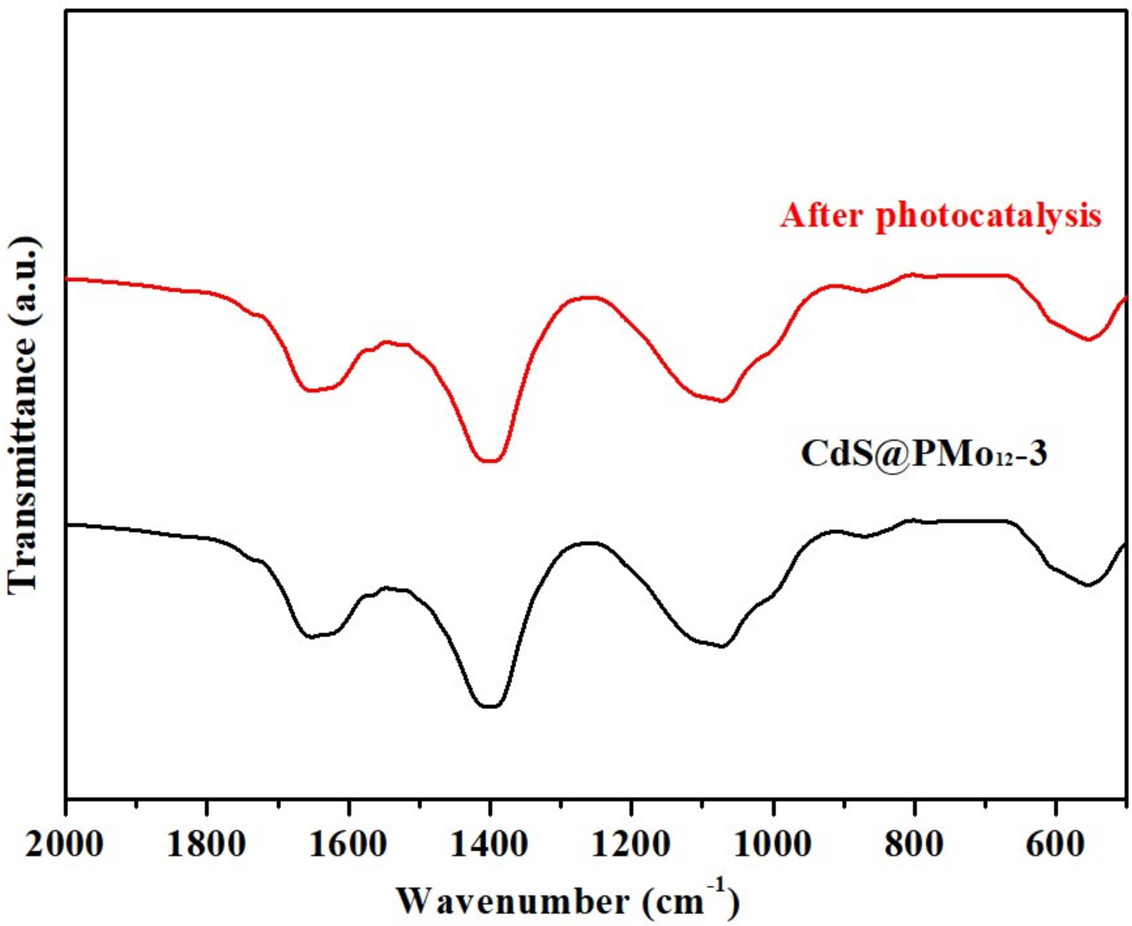

Figure S15. FT-IR spectra of $CdS@PMo_{12}$-3 before and after the photocatalytic H_2 evolution.

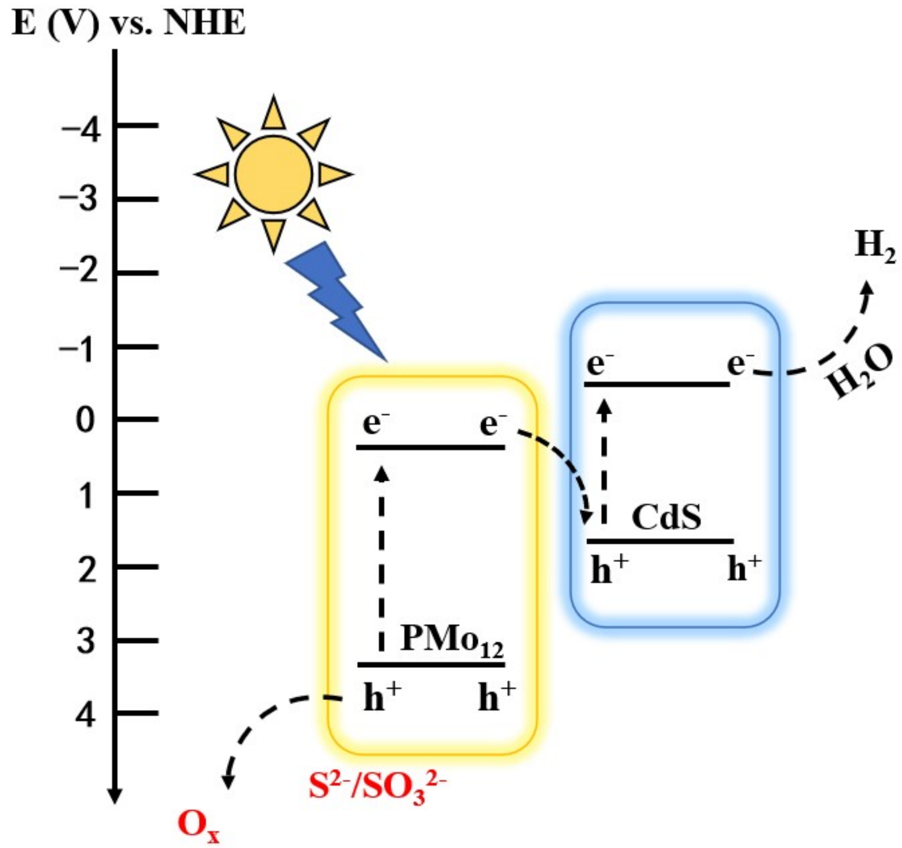

Figure S16. Proposed possible mechanism schematic of CdS@PMo_{12} composite.

Table S1. ICP-MS results of CdS@PMo_{12}.

Compounds	PMo_{12} (mg)	Elements Mo (wt%)
CdS@PMo_{12}-1	10	0.7
CdS@PMo_{12}-2	30	1.1
CdS@PMo_{12}-3	50	1.8
CdS@PMo_{12}-4	70	2.7

Table S2. A comparison of the H_2-production rates of the POM-based photocatalysts and most CdS-based photocatalysts.

Photocatalyst	Amounts of catalyst(mg)	Activity (mmol h^{-1} g^{-1})	Refs
CdS@PMo_{12}-3	2	5.7	This Work
CdS-P_5W_{30}	50	1.9	1
$Ti_3C_2T_x$/CdS	20	0.8	2
CdS-NiE-350	100	4.3	3
NiS/CdS	30	2.2	4
M–G/CdS	100	2.3	5
Au–Pt–CdS	50	0.8	6
CdS-NRs/NMOF-Ni	50	4.5	7
Ag_2S/CdS	50	0.7	8
MnO_2 @CdS	5	3.9	9
$P_2W_{15}V_3$@MIL-101	3	0.9	10
Co-POM	1	2.0	11

References

1. H. Chen, Y. Cao, R. Wang, Y. Li, M. Liu, L. Zhang and W. You, Enhanced photocatalytic performance in preyssler-type P_5W_{30}-CdS nanohybrids synthesized by l-cystine-mediated hydrothermal assembly, *Int. J. Hydrogen Energy,* 2019, **44**, 13052-13060.

2. Y. Yang, D. Zhang and Q. Xiang, Plasma-modified Ti_3C_2Tx/CdS hybrids with oxygen-containing groups for high-efficiency photocatalytic hydrogen production. *Nanoscale,* 2019, **11**, 18797-18805.

3. G. Zhao, Y. Sun, W. Zhou, X. Wang, K. Chang, G. Liu, H. Liu, T. Kako and J. Ye, Superior Photocatalytic H_2 Production with Cocatalytic Co/Ni Species Anchored on Sulfide Semiconductor, *Adv. Mater.,* 2017, **29**, 1703258.

4. W. Zhang, Y. Wang, Z. Wang, Z. Zhong and R. Xu, Highly efficient and noble metal-free NiS/CdS photocatalysts for H_2 evolution from lactic acid sacrificial solution under visible light, *Chem. Commun.,* 2010, **46**, 7631-7633.

5. M. Liu, F. Li, Z. Sun, L. Ma, L. Xu and Y. Wang, Noble-metal-free photocatalysts MoS_2-graphene/CdS mixed nanoparticles/nanorods morphology with high visible light efficiency for H_2 evolution, *Chem. Commun.,* 2014, **50**, 11004-11007.

6. L. Ma, K. Chen, F. Nan, J. H. Wang, D. J. Yang, L. Zhou and Q. Q. Wang, Improved Hydrogen Production of Au-Pt-CdS Hetero-Nanostructures by Efficient Plasmon-Induced Multipathway Electron Transfer, *Adv. Funct. Mater.,* 2016, **26**, 6076-6083.

7. H. Yang, C. Yang, N. Zhang, K. Mo, Q. Li, K. Lv, J. Fan and L. Wen, Drastic promotion of the photoreactivity of MOF ultrathin nanosheets towards hydrogen production by deposition with CdS nanorods, *Appl. Catal., B,* 2021, **285**, 119801.

8. C. Lu, S. Du, Y. Zhao, Q. Wang, K. Ren, C. Li and W. Dou, Efficient visible-light photocatalytic H_2 evolution with heterostructured Ag_2S modified CdS nanowires, *RSC Adv.,* 2021, **11**, 28211-28222.

9. S. Zulfiqar, S. Liu, N. Rahman, H. Tang, S. Shah, X. H. Yu and Q. Q. Liu, Construction of S-scheme MnO_2@CdS heterojunction with core–shell structure as H_2-production photocatalyst, Rare Met., 2021, 40, 2381-2391.

10. W. Sun, B. An, B. Qi, T. Liu, M. Jin and C. Duan, Dual-Excitation Polyoxometalate-Based Frameworks for One-Pot Light-Driven Hydrogen Evolution and Oxidative Dehydrogenation, *ACS Appl. Mater. Interfaces.,* 2018, **10**, 13462-13469.

11. H. Li, S. Yao, H. L. Wu, J. Y. Qu, Z. M. Zhang, T. B. Lu, W. Lin and E. B. Wang, Charge-regulated sequential adsorption of anionic catalysts and cationic photosensitizers into metal-organic frameworks enhances photocatalytic proton reduction, *Appl. Catal., B,* 2018, **224**, 46-52.